A method to estimate automotive powertrain inertia properties using operational vibrations

Méthode de détermination des propriétés d'inertie d'un GMP à partir de vibrations opérationnelles

F. Barillon[1], L. Polac[2] et C. Thévenard[3]

1 Service Simulation Numérique, Renault SA – 1, avenue du Golf 78288 Guyancourt, France, e-mail : franck.barillon@renault.com

2 Service Ingénierie Cadrage Amont GMP, Renault SA – 1, allée Cornuel, 91510 Lardy, France, e-mail : laurent.polac@renault.com

3 Service Prestations acoustiques et vibrations, Renault SA – Centre Technique d'Aubevoye 27940 Aubevoye, France, e-mail : christophe.thevenard@renault.com

Résumé

Aujourd'hui la réduction des émissions polluantes, de la consommation et de la masse des véhicules constitue un enjeu majeur pour l'industrie automobile et amène au développement de moteurs à 3 cylindres. Ces moteurs sont très différents des moteurs à 4 cylindres du point de vue vibratoire car leur fréquence de fonctionnement se situe dans la plage des modes de corps solides du moteur. La prédiction de ces modes par le calcul repose donc sur la bonne connaissance des propriétés d'inertie du moteur : position du centre de gravité, masse et matrice d'inertie. Les méthodes classiques d'estimation des propriétés d'inertie d'un moteur (pendule ou ligne de masse) sont difficiles à appliquer et imprécises car n'étant pas réalisées en environnement véhicule. Cet article présente une méthode originale de détermination des inerties d'un moteur à partir des vibrations opérationnelles. Cette méthode sera validée numériquement avant d'être appliquée expérimentalement. En préambule, une discussion sur la prise en compte du balourd statique résiduel est proposée, qui peut rendre la méthode encore plus précise.

Mots clés : Automobile, Moteurs, 3 cylindres, Inerties, In Situ.

Abstract

Today, fuel consumption and weight reduction issues in automotive industry leads to downsizing with the development of 3-cylinder engines. These powertrains present high level of idle vibrations due to the excitation of engine rigid body modes. Inertia properties thus need to be well known to be reintroduced into finite element analysis.

Pendulum method and modal method are well-known methods to estimate the inertia tensor of a solid, but reveals quite difficult and time consuming to be applied in situ on a complete vehicle. This paper proposes an original method to estimate the inertia properties (c.o.g. position, mass and inertia tensor) of a powertrain using operational vibrations. Both numerical and test results are presented showing the efficiency of the method. Previously to this method, a quick analysis of first engine order vibrations is conducted in order to estimate real unbalance so that the inertia properties should be more accurately evaluated.

.

Keywords : *Automotive, Powertrain, 3-cylinder, Inertia, In Situ.*

1 Introduction

Today, reducing the weight of powertrains and CO2 emission lead most of car manufacturers to the development of 3-cylinders engines. These kinds of powertrain differ from usual 4-cylinders engines presenting very low frequency excitations in the range of rigid body modes of the powertrain. It is thus needed to get accurate inertia properties of the powertrain to simulate engine vibrations in this frequency range during the development phase. Moreover, a good knowledge of inertia properties in mechanical units is required particularly in designing and refining powertrain mountings, or in estimating and optimizing NVH of the powertrain itself.

Considering the mass size of this type of unit, any handling requires means using a handling device and it takes up a lot of time. For this reason amongst others, the standard measuring methods of inertia properties in mechanical units are laborious and expensive. We therefore tried to get around this problem by, as much as possible, taking the measurements in running conditions which are carried out during the development and NVH refinement of the powertrain.

The original method described below (in situ method) uses the rigid body mechanics applied to the vibrations of the powertrain at low-frequencies and requires a minimum of input data in addition to the measurements taken under running conditions. The other advantage of this method is to measure the powertrain inertias without any handling conditions that can lead to inertia modifications, taking into account every subsystem connected to the engine (e.g. driveshaft, accessories).

In this paper we will first briefly describe engine idle vibrations issues and focus on 3-cylinders powertrain concerns and specificities. Second part of this paper presents existing methods to measure powertrain inertia properties. Finally we will describe the proposed new in-situ method that will be validated both numerically and experimentally.

2 Idle vibrations global overview

Idle vibrations represent an important NVH performance concern for Renault customers' comfort and quietness. Idle vibrations are generated by engine excitations transmitted to the car body in low frequencies. At idle rpm, excitations are stationary and can be expressed as harmonics of the engine rotational speed. In this part of the paper, we will set the main concerns about idle vibrations performance and describe theoretical concerns and mathematical forms that will be useful in the following.

2.1 Usual engine architecture

Usual engines are connected to the car body by rubber engine mounts whose main function is to isolate car passengers from engine vibrations represented on Figure 1. Main engine mounts are:

- Gearbox mount (LH side)
- Engine mount (RH side)
- Lower torque rod
- Upper torque rod for most powerful engines with high torque levels.

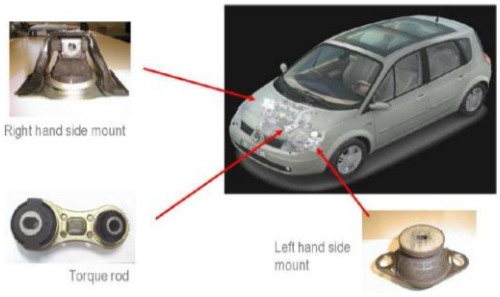

Fig. 1. Common engine architecture.

Figure 2 describes usual modal allocations in a complete vehicle. Just after vehicle rigid body modes on the tires, occur engine rigid body modes. They correspond to the 6 rigid body modes (6 degrees of freedom) of the engine connected to the car body by engine mounts most of the time located between 5 Hz and 20 Hz. After 30 Hz, body elastic modes appear with global torsion, bending and accessories modes. Usual 4 –cylinders excitations are set between 20 Hz and 30 Hz, not to excite engine rigid body modes neither global body modes.

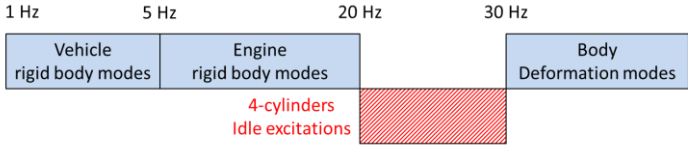

Fig. 2. Global overview of vehicle modes.

Engine excitations names depend on their direction. Figure 3 presents the nomenclature that will be used in this paper. Excitations fully depend on powertrain type and are divided in:

- Gas excitation due to internal combustion (depending on engine load)
- Inertia (mechanical) excitation due to the rotation of crankshaft and all moving parts (increases with engine rpm)

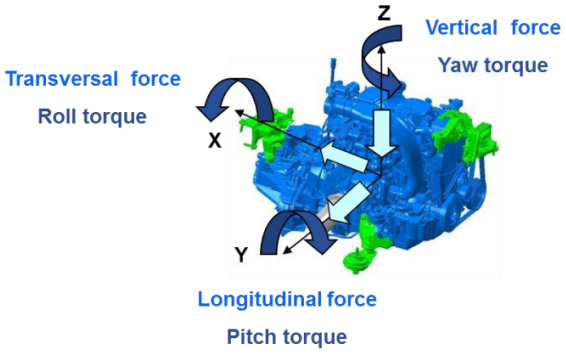

Fig. 3. Engine excitations tensor.

In this paper, engine excitation tensor is expressed as the sum of all harmonic tensors written (eq. 1).

$$\begin{bmatrix} Fx & Mx \\ Fy & My \\ Fz & Mz \end{bmatrix} = \sum_{i=1}^{harmonics} \begin{bmatrix} Fx^{Hi} & Mx^{Hi} \\ Fy^{Hi} & My^{Hi} \\ Fz^{Hi} & Mz^{Hi} \end{bmatrix}_{gas} + \begin{bmatrix} Fx^{Hi} & Mx^{Hi} \\ Fy^{Hi} & My^{Hi} \\ Fz^{Hi} & Mz^{Hi} \end{bmatrix}_{inertia} \quad \text{(eq. 1)}$$

2.2 3-cylinders idle excitations

As illustrated Figure 4, 3-cylinders engine excitations are lower in frequency, directly in the frequency range of engine rigid body modes. In the development phase, it is thus needed to have good estimation of the frequency of these modes, directly linked to bushing stiffness and inertia properties of the powertrain (inertia tensor, mass and center of gravity position).

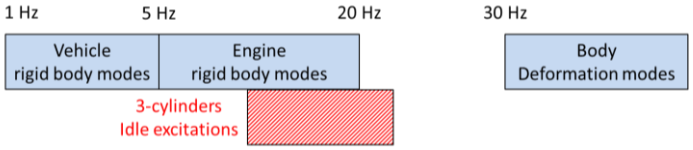

Fig. 4. Global overview of vehicle modes.

2.2.1 Gas forces

Due to the fuel internal combustion, gas excitation tensor at idle can be reduced to roll torque along harmonic 1.5 (3 explosions every 2 crankshaft cycles) expressed equation 2.

$$\begin{bmatrix} Fx & Mx \\ Fy & My \\ Fz & Mz \end{bmatrix}_{gas} \approx \begin{bmatrix} 0 & 0 \\ 0 & M_y^{H1.5} \\ 0 & 0 \end{bmatrix} \approx \begin{bmatrix} 0 & 0 \\ 0 & \left|M_y^{H1.5}\right|\cos\left(1.5\omega t + \varphi_y^{H1.5}\right) \\ 0 & 0 \end{bmatrix} \quad \text{(eq. 2)}$$

where ω represents the engine rotational speed in rad.s^{-1}.

2.2.2 Inertia forces

Combustion into cylinders leads to the movement of pistons and crankshaft. Inertia excitation tensor can be reduced as equation 3 for nominal crankshaft balancing since there is no residual static unbalance. Main harmonics for 3-cylinder powertrains are harmonic 1 and 2. Main torques are pitch and yaw.

$$\begin{bmatrix} Fx & Mx \\ Fy & My \\ Fz & Mz \end{bmatrix}_{inertia} \approx \begin{bmatrix} 0 & M_x^{H1} + M_x^{H2} \\ 0 & 0 \\ 0 & M_z^{H1} \end{bmatrix} \approx \begin{bmatrix} 0 & \left|M_x^{H1}\right|\cos\left(\omega t + \varphi_x^{H1}\right) + \left|M_x^{H2}\right|\cos\left(2\omega t + \varphi_x^{H2}\right) \\ 0 & 0 \\ 0 & \left|M_z^{H1}\right|\cos\left(\omega t + \varphi_z^{H1}\right) \end{bmatrix} \quad \text{(eq. 3)}$$

Unfortunately, residual static unbalance may be not negligible in real life. Then, equation 3 must be replaced by equation 3bis

$$\begin{bmatrix} Fx & Mx \\ Fy & My \\ Fz & Mz \end{bmatrix}_{inertia} \approx \begin{bmatrix} B\cos\left(\omega t + \varphi^B\right) & \left|M_x^{H1}\right|\cos\left(\omega t + \varphi_x^{H1}\right) + \left|M_x^{H2}\right|\cos\left(2\omega t + \varphi_x^{H2}\right) \\ 0 & 0 \\ B\sin\left(\omega t + \varphi^B\right) & \left|M_z^{H1}\right|\cos\left(\omega t + \varphi_z^{H1}\right) \end{bmatrix} \quad \text{(eq. 3bis)}$$

Where ω represents the engine rotational speed, $B = \omega^2$ static unbalance and φ^B is the phase angle of the residual static unbalance. Static unbalance may be approximately assessed by the mean of abacuses (see example below) obtained by assuming initial values for center of gravity location and Inertia matrix. Then, an iterative process may achieve accurate final values for center of gravity location and Inertia matrix since mass is preferably obtained by weighing. Example of abacus for a given static unbalance amplitude, a given powertrain mass, inertia and cog location is given Figure 5, where ||SM1X|| 0° means amplitude of gearbox bracket vibration at 1st harmonic for $\varphi^B = 0°$

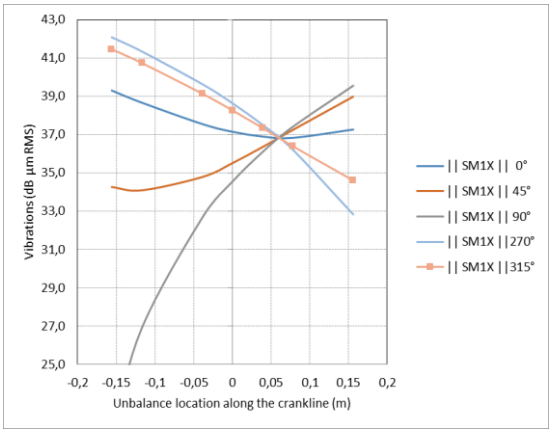

Fig. 5. Example of static unbalance on Gearbox bracket 1st harmonic vibration in X direction.

By the mean of several abacuses showing gearbox and engine bracket 1st harmonic vibration in X and Z directions for several unbalance amplitudes, it is possible to approximate static unbalance amplitude, location and phase by updating computed bracket vibration on measured bracket vibration.

Table 1 presents the corresponding excitation frequencies for a 3-cylinders powertrain for usual idle rpm. We can easily see that the excitation frequency is in the range of the rigid body modes of the engine.

RPM	650 – 900 rpm
Harmonic 1	10.8 Hz – 15 Hz
Harmonic 1.5	16.3 Hz – 22.5 Hz
Harmonic 2	21.7 Hz – 30 Hz

Tab. 1. 3-cylinders excitation frequencies.

3 State of the art to determine inertia properties

Up to now, 2 kinds of methods are used to determine experimentally inertia properties: inertia matrix, center of gravity (c.o.g.) location and mass.

3.1 Pendulum method

The first method is known as the pendulum test: by hanging the structure freely in 2 directions at least, the c.o.g. is obtained. Then, to determine inertia tensor $\overline{\overline{I}}$ components (6 unknown values as this matrix is symmetrical) the pendulum test must be done in 6 different conditions at least: torsional pendulum period combined with torsional stiffness of the suspension system leads to inertia momentum.

To locate its c.o.g., the structure is suspended by at least 2 points according to the diagram described in Figure 6. The c.o.g. position is obtained by intersecting the 2 vertical straight lines located on the reference mark of the structure. The quality of the result is linked to the amount of care taken in locating the intersection points for each of the vertical lines with the surface of the structure. To carry out this task, using laser beams is strongly recommended. In this case, the precision obtained is around 5 mm.

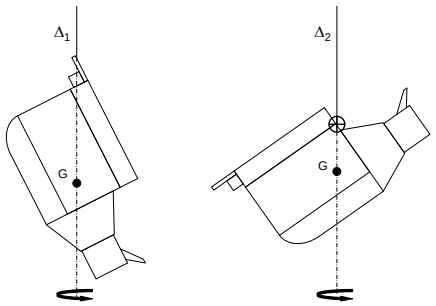

Fig. 6. Pendulum method.

To determine the inertia tensor $\overline{\overline{I}}$, which contains 6 unknown quantities since it is symmetrical, the torsion pendulum period is measured in at least 6 configurations as described in Figure 5. Six straight lines Δ_i passing through the engine center of gravity are obtained by suspending the engine in 6 different conditions. Guiding coefficients (u_i, v_i, w_i) are related by equation 4.

$$u_i^2 + v_i^2 + w_i^2 = 1 \qquad \text{(eq. 4)}$$

Equation 5 gives the inertia I_{Δ_i} of the structure in relation to Δ_i

$$I_{\Delta_i} = \begin{Bmatrix} u_i \\ v_i \\ w_i \end{Bmatrix}^T \overline{\overline{I}} \begin{Bmatrix} u_i \\ v_i \\ w_i \end{Bmatrix} \quad \text{(eq. 5)}$$

By noting T_i (resp. C_i) the torsion period (resp. the stiffness) of measurement number i, I_{Δ_i} is also expressed as equation 6 that can be combined to equation 5 to provide system of equations 7. Therefore, provided that the 6 pendulum directions are carefully chosen, the system is invertible and the inversion gives a particularly precise result given that the conditioning number of the system is weak. This first method is very laborious and time consuming but it can achieve reliable accuracy if it is cautiously carried out.

$$T_i = 2\pi\sqrt{\frac{I_{\Delta i}}{C_i}} \quad \rightarrow \quad I_{\Delta i} = \frac{C_i T_i^2}{4\pi^2} \quad \text{(eq. 6)}$$

$$\begin{Bmatrix} u_i \\ v_i \\ w_i \end{Bmatrix}^T \overline{\overline{I}} \begin{Bmatrix} u_i \\ v_i \\ w_i \end{Bmatrix} = \frac{C_i T_i^2}{4\pi^2} \quad i = 1 \ldots 6 \quad \text{(eq. 7)}$$

One variant of the pendulum method is the rolling plate method using a tilt system avoiding any handling of the structure, represented in Figure 7. For at least 6 configurations, the straight line passing through engine center of gravity Δ and the plate direction Δ' are measured. Equation set 8 is then similar to classic pendulum method by removing inertia of the rolling plate.

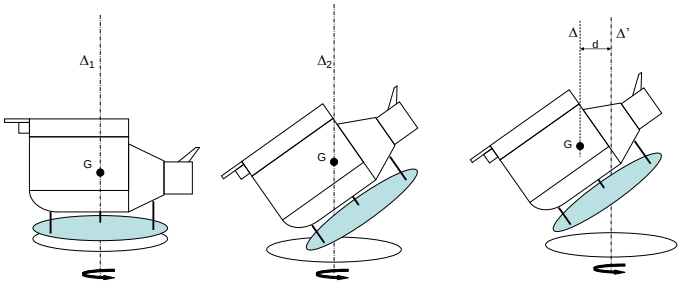

Fig. 7. Rolling plate method.

$$\begin{Bmatrix} u_i \\ v_i \\ w_i \end{Bmatrix}^T \overline{\overline{I}} \begin{Bmatrix} u_i \\ v_i \\ w_i \end{Bmatrix} = \frac{C_i T_i^2}{4\pi^2} - I_{plate} - Md(G,\Delta'_i)^2 \quad i = 1 \ldots 6 \quad \text{(eq. 8)}$$

Where I_{plate}, M and $d(G,\Delta'_i)$ represent the known inertia and mass of the plate and the distance between the engine center of gravity and Δ'_i respectively.

The pendulum method according to 6 directions usually requires at least three additional brackets to be fitted because a powertrain only has 3 connecting brackets to the car body. The work is considerable but the accuracy is generally good (5 mm on c.o.g. location error and less than 10% on principal Inertia moments). In the variant using an oscillating plate, the work is less laborious but the accuracy is not so good because of dealing with differences in measurements and that the position of G is already marred with an uncertainty. The overall duration is about 2 weeks.

3.2 Modal method

The second method is an alternative to the pendulum test and it is known as a modal test and mass line method. It is based on frequency response function (FRF) measurements on the structure in free-free conditions (by the mean of a very flexible suspension system). The excitation can be introduced either by an impact hammer or a shaker. The second method is rather effective but not as accurate as the first one because of additional uncertainties induced by excitation (amplitude and direction) and response.

The analyzed structure is suspended very flexibly to obtain the best free-free conditions as illustrated in Figure 8. Excitations are generated by a hammer or by a shaker. The inertia characteristics are determined by calculating the properties of a rigid body based on the measured FRF (frequency response functions). Points A and B are located on the structure, G represents the engine c.o.g.

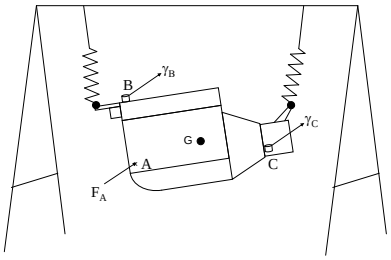

Fig. 8. Experimental set-up for modal method.

Frequency range for analysis is carefully chosen after the first rigid body modes of the engines on its suspension and before its first elastic mode, so that the behavior can be considered as mass and inertia as illustrated Figure 9.

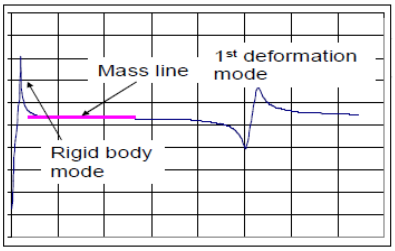

Fig. 9. Mass line frequency range using modal method.

Writing classic equations for solids gives equation 9

$$\overrightarrow{V_B} = \overrightarrow{V_G} + \overrightarrow{\Omega} \wedge \overrightarrow{GB} \qquad \text{(eq. 9)}$$

Where $\overrightarrow{V_B}$, $\overrightarrow{V_G}$ and $\overrightarrow{\Omega}$ represent the speed of point B, point G and the rotational speed of the structure, respectively. By derivating equation 9, we obtain equation 10

$$\overrightarrow{\gamma_B} = \overrightarrow{\gamma_G} + \overrightarrow{\Omega'} \wedge \overrightarrow{GB} + \overrightarrow{\Omega} \wedge \frac{d\overrightarrow{GB}}{dt} = \overrightarrow{\gamma_G} + \overrightarrow{\Omega'} \wedge \overrightarrow{GB} + \overrightarrow{\Omega} \wedge \left(\overrightarrow{\Omega} \wedge \overrightarrow{GB}\right) \qquad \text{(eq. 10)}$$

Where $\overrightarrow{\gamma_B}$, $\overrightarrow{\gamma_G}$ and $\overrightarrow{\Omega'}$ represent the acceleration of point B, point G and the rotational acceleration of the structure, respectively. Since $\left\|\overrightarrow{\Omega'} \wedge \overrightarrow{GB}\right\| >> \left\|\overrightarrow{\Omega} \wedge \left(\overrightarrow{\Omega} \wedge \overrightarrow{GB}\right)\right\|$ in general, we obtain equation 11.

$$\overrightarrow{\gamma_B} = \overrightarrow{\gamma_G} + \overrightarrow{\Omega'} \wedge \overrightarrow{GB} \qquad \text{(eq. 11)}$$

Then, applying dynamic fundamental principle provides set of equation 12

$$\begin{cases} \overrightarrow{\gamma_G} = \dfrac{\overrightarrow{F_A}}{m} \\ \overline{\overline{I}}\,\overrightarrow{\Omega'} = \overrightarrow{GA} \wedge \overrightarrow{F_A} \end{cases} \quad \text{(eq. 12)}$$

Where $\overrightarrow{F_A}$, m and $\overline{\overline{I}}$ represent the force (hammer) applied on the structure, total mass of the structure and symmetrical inertia tensor $\overline{\overline{I}}$ respectively..

Replacing equation 12 into equation 11, provides equation set 13 involving $\overline{\overline{I}}$, m and G and known quantities.

$$\left[\overline{\overline{I}}^{-1} \left(\overrightarrow{GA} \wedge \overrightarrow{F_A} \right) \right] \wedge \overrightarrow{GB} = \overrightarrow{\gamma_B} - \frac{\overrightarrow{F_A}}{m} \quad \text{(eq. 13)}$$

Equation set 13 provides 6 equations to find 10 unknowns (6 for $\overline{\overline{I}}$, 1 for m , 3 for G coordinates). To get additional equations, it is thus needed to excite the engine at different locations. Typically, the structure being instrumented using at least 3 three-dimensional acceleration sensors, it is usually enough to excite the structure with 2 different force directions or in 2 different points.

As a conclusion, where a modal analysis is already planned, extracting the inertia properties has a low marginal cost. The accuracy is good so long as the force is known in amplitude, phase and in direction and that its application point is well localized. On the other hand, where a modal analysis is not already planned, the cost of extracting the inertia properties is around that of a modal analysis if we take into account the work required to empty the powertrain of its fluids and to suspend it. The overall duration is about a week.

4 New in situ method

The new experimental in situ method described hereinafter is based on the fact that, particularly with reciprocating engines, some harmonic vibrations from the powertrain under running conditions show constant displacement amplitudes at a rather large engine speed range. These constant values are related to inertia properties of powertrain structure and mass and kinematic properties of moving parts. Then, provided that stroke, piston mass, con rod c.o.g. and con rod mass and length are known, powertrain inertia properties may be estimated with reliable accuracy in situ (powertrain installed in the car) or on a powertrain test bench during a classical NVH or reliability test.

Experimental set up is illustrated Figure 10. G represents the engine c.o.g. A, B and C are chosen at extreme locations on the engine in order to get maximum displacements and avoid symmetry axes.

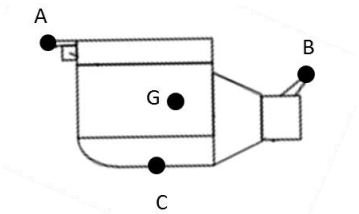

Fig. 10. In-situ method instrumentation set up.

Experimental set up consists in measuring A, B and C points vibrations during an engine rpm sweep in idle conditions. Rpm range of interest is chosen after the 6th rigid body mode of the engine (around 20 Hz) and before the first elastic mode of the powertrain (around 200Hz). Rpm range of interest can be chosen between 1500 and 4500 rpm. In this rpm range, engine behavior corresponds to a mass/inertia system excited by gas and inertia forces and torques. Figure 11 illustrates powertrain vibrations during an idle sweep between 600 rpm and 5000 rpm.

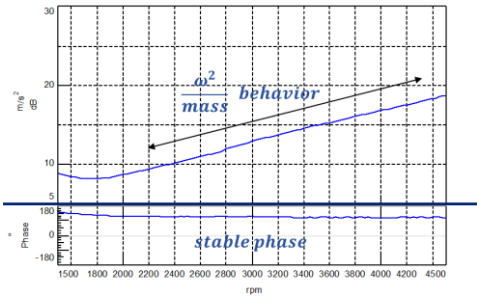

Fig. 11. Measured engine mount vibrations during a rpm sweep – Harmonic 1.

4.1 Global method

In this section we will describe general equations to determine inertia properties (inertia matrix, mass and c.o.g. position) on an engine using operational vibrations.

4.1.1 Estimation of inertia tensor

Applying equation 11 provides equation set 14 and 14bis.

$$\begin{cases} \overrightarrow{\gamma_B} = \overrightarrow{\gamma_G} + \overrightarrow{\Omega'} \wedge \overrightarrow{GB} \\ \overrightarrow{\gamma_A} = \overrightarrow{\gamma_G} + \overrightarrow{\Omega'} \wedge \overrightarrow{GA} \end{cases} \quad \text{(eq. 14)}$$

$$\begin{cases} \overrightarrow{\gamma_A} - \overrightarrow{\gamma_B} = \overrightarrow{AB} \wedge \overrightarrow{\Omega'} \\ \overrightarrow{\gamma_A} - \overrightarrow{\gamma_C} = \overrightarrow{AC} \wedge \overrightarrow{\Omega'} \end{cases} \quad \text{(eq. 14bis)}$$

That can be expressed under matrix form 15.

$$\begin{Bmatrix} \overrightarrow{\gamma_A} - \overrightarrow{\gamma_B} \\ \overrightarrow{\gamma_A} - \overrightarrow{\gamma_C} \end{Bmatrix} = \overline{\overline{\Lambda \overrightarrow{\Omega'}}} \begin{Bmatrix} \overrightarrow{AB} \\ \overrightarrow{AC} \end{Bmatrix} \quad \text{(eq. 15)}$$

Where $\overline{\overline{\Lambda \overrightarrow{\Omega'}}}$ represents the vector product operator under matrix form. We are then able to compute rotational acceleration of the engine since point A and B vibrations and point A and B locations are known.

Second step of the method consists in applying dynamic fundamental principle to the engine for each harmonic giving a complete set of equations 16 allowing determination of inertia matrix $\overline{\overline{I}}$ since engine torques are known.

$$\boxed{\overline{\overline{I}} \overrightarrow{\Omega} = \sum_{Torques} \overrightarrow{M_{ext}}} \quad \text{(eq. 16)}$$

4.1.2 Estimation of c.o.g. position

Applying dynamic fundamental principle to the engine provides equation 17.

$$\overrightarrow{\gamma_G} = \frac{\vec{F}}{m} \quad \text{(eq. 17)}$$

Since vectors are collinear, we can write equation 18.

$$\overrightarrow{\gamma_G} \wedge \vec{F} = \vec{0} \quad \text{(eq. 18)}$$

Introducing equation 18 into equation 14 provides equations 19 and 20.

$$\overrightarrow{\gamma_G} = \overrightarrow{\gamma_A} + \overrightarrow{GA} \wedge \vec{\Omega}' \quad \text{(eq. 19)}$$

$$\left(\overrightarrow{\gamma_A} + \overrightarrow{GA} \wedge \vec{\Omega}'\right) \wedge \vec{F} = \vec{0} \quad \text{(eq. 20)}$$

Exploiting vector decomposition referring to global coordinate center O provides equations 21 and 22.

$$\overrightarrow{GA} = \overrightarrow{GO} + \overrightarrow{OA} \quad \text{(eq. 21)}$$

$$\boxed{\left(\overrightarrow{OG} \wedge \vec{\Omega}'\right) \wedge \vec{F} = -\left(\overrightarrow{\gamma_A} + \overrightarrow{OA} \wedge \vec{\Omega}'\right) \wedge \vec{F}} \quad \text{(eq. 22)}$$

Equation 21 provides a complete set of equation to determine engine c.o.g. coordinates $\overrightarrow{OG}$.

4.1.3 Estimation of the mass

Starting from equations 17 and 19 allows to express the total mass of the engine as equation 23

$$\boxed{m = \frac{\left\|\vec{F}\right\|}{\left\|\overrightarrow{\gamma_A} + \overrightarrow{GA} \wedge \vec{\Omega}'\right\|}} \quad \text{(eq. 23)}$$

4.2 Application to 3-cylinders powertrain

4.2.1 Estimation of inertia tensor

After determining the rotational acceleration of the engine for each harmonic, equation 16 can be expressed as followed, based on engine torques expression 2 and 3 for 3-cylinders engines.

For harmonic 1, harmonic 1.5 and harmonic 2:

$$\overrightarrow{\overline{I}\vec{\Omega}'} = \begin{Bmatrix} M_x^{H1} \\ 0 \\ M_z^{H1} \end{Bmatrix} \quad \overrightarrow{\overline{I}\vec{\Omega}'} = \begin{Bmatrix} 0 \\ M_y^{H1.5} \\ 0 \end{Bmatrix} \quad \overrightarrow{\overline{I}\vec{\Omega}'} = \begin{Bmatrix} M_x^{H2} \\ 0 \\ 0 \end{Bmatrix} \quad \text{(eq. 24, eq. 25, eq. 26)}$$

4.2.2 Estimation of c.o.g. position

For c.o.g. location estimation, equation 22 cannot be applied directly because $\vec{F} = \vec{0}$ for 3-cylinders since only torques are applied. Applying equation 17 provides in this case $\overrightarrow{\gamma_G} = \vec{0}$ that can be reintroduced into equation 19, using decomposition 21 giving equation 27.

$$\overrightarrow{OG} \wedge \vec{\Omega}' = \overrightarrow{\gamma_A} + \overrightarrow{OA} \wedge \vec{\Omega}' \qquad \text{(eq. 27)}$$

4.2.3 Estimation of the mass

Since $\vec{F} = \vec{0}$ for a 3-cylinder engine, it is impossible to get the engine mass using equation 23. To get the engine mass in-situ, we recommend to proceed in-situ modal testing that can give accurate results. It is of course possible to weight the engine !

5 Numerical validation

5.1 Finite element model description

To validate this new in-situ method numerically, we used a finite element model of a complete vehicle introducing a rigid model of the engine represented by its mass and inertia matrix linked to the car body with engine mounts represented with bushings. Numerical model is presented Figure 12.

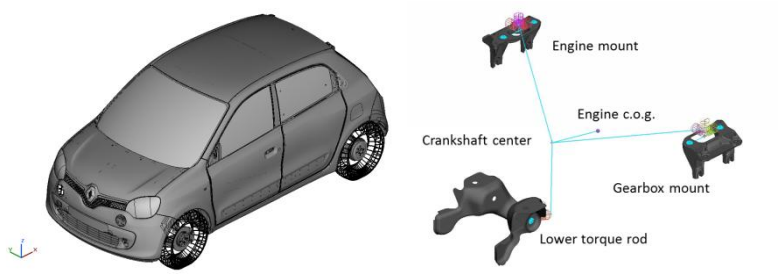

Fig. 12. Finite element model of complete vehicle and 3-cylinder engine.

Theoretical harmonic excitations were applied to the crankshaft including both gas and inertia torques increasing with rpm. Points A, B and C were chosen at engine mounts brackets locations. Idle sweep is calculated from 1500 rpm to 4500 rpm. Since the engine is only represented by its mass an inertia matrix, no elastic powertrain modes can occur.

5.2 Inertia properties estimation

For every rpm, equations 15, 16 and 27 are solved to get an estimation of the c.o.g. coordinates and all the inertia terms whose expression is given equation 28.

$$\overline{\overline{I}} = \begin{bmatrix} I_{xx} & -I_{xy} & -I_{xz} \\ -I_{xy} & I_{yy} & -I_{yz} \\ -I_{xz} & -I_{yz} & -I_{zz} \end{bmatrix} \qquad \text{(eq. 28)}$$

Figure 13 represents the convergence of these inertia properties with engine rpm. Phase of the terms are equaled to 0° or 180° since inertia terms are real. We can easily see a fast convergence of the equations since we have a perfect mass/inertia behavior in the calculation, providing remarkable stable phases and amplitudes of vibrations for points A, B and C.

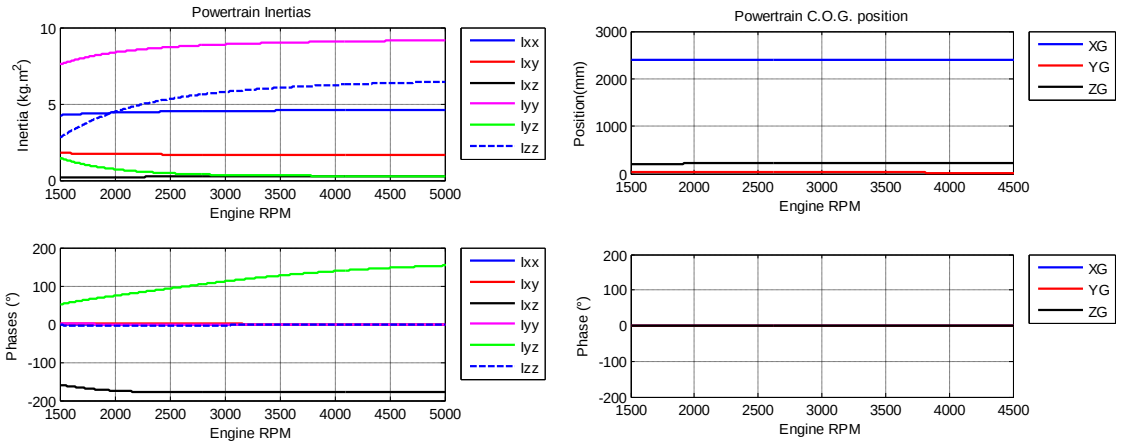

Fig. 13. Estimated inertias with engine rpm.

Table 2 presents the error of estimation at 4500 rpm for the 6 inertia terms of matrix $\overline{\overline{I}}$ and for the c.o.g. coordinates comparing to input datas that were used, showing accuracy of the method. We can notice that terms Izz and Iyz present slow amplitude convergence that can be explained because of low level of yaw torque that were used in the numerical simulation on harmonic 1. We can also notice that for low amplitudes inertia terms, convergence of phases is slow.

Inertia terms	Estimation error (%)
Ixx	0.75
Iyy	1.57
Izz	5.33
Iyz	5.27
Ixz	0.99
Ixy	1.40
C.O.G. coordinates	**Estimation error (%)**
X	0.01
Y	1.31
Z	0.20

Tab. 2. Estimated inertia properties vs. Input.

6 Experimental validation

6.1 Experimental set up

For experimental testing of the method, we measured a 3-cylinder engine operational vibrations and cylinder pressure during a rpm sweep in idle conditions. Set-up environment is a test bench including driveshafts and engine accessories to get close conditions to real vehicle. The engine is linked to the test bench with 3 engine rubber mounts. Any handling is used in all this experimental phase. Points A, B and C are chosen at engine mount brackets location because these points are usually accessible. Figure 14 represents the experimental set-up.

Fig. 14. In-situ measurement on the test bench with driveshaft suspension system.

6.2 In situ inertia properties estimation

For this application, initial positions of points A, B and C are known from architecture of the vehicle. For each rpm, inertia terms and c.o.g were computed. Figure 15 illustrates convergence of these quantities with respect to rpm. We can see that accordingly to results presented on Figure 13, inertia terms present good convergence except inertia terms Izz and Iyz . Nevertheless, Izz term present a flat curve between 2500 rpm and 3500rpm allowing estimation of its amplitude. We can also notice that after 4000 rpm, perturbation is due to first elastic mode of the powertrain. Estimation of c.o.g. location shows good convergence in amplitude. Phase convergence is slower for low amplitude terms. These results show that in-situ method allows determining real inertia properties term of the powertrain.

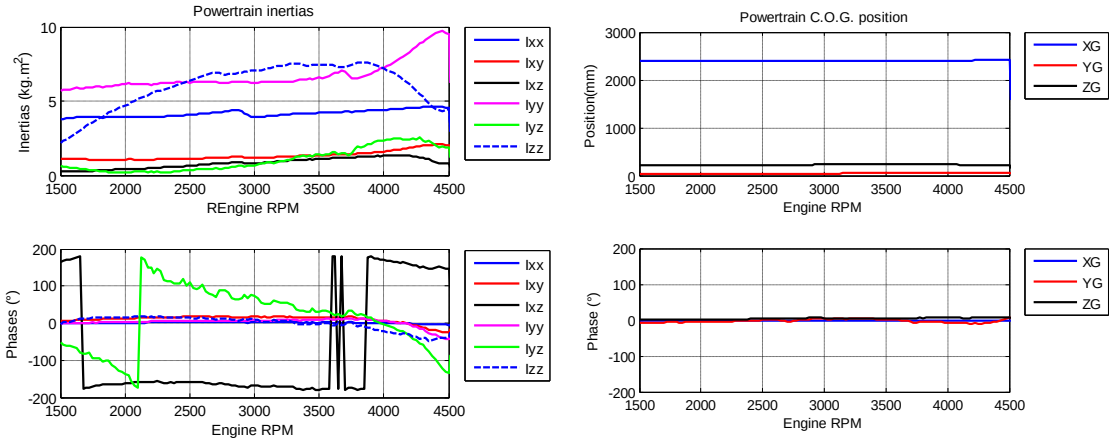

Fig. 15. Measured inertias with engine rpm.

6.3 Reintroducing inertia properties into finite element models

After estimating inertia properties of the engine experimentally, last part of the validation consists in reintroducing these inertia properties into a finite element simulation in order to compute vibrations. Figure 16 and Figure 17 present a comparison between measurements on the test bench and computation after introducing measured inertia properties (inertia tensor and c.o.g. coordinates) into a finite element model excited by theoretical engine excitation tensor on harmonic 1, 1.5 and 2. These results show good correlation between calculations and measurements in the mass behavior rpm range, showing that inertia properties estimation was sufficient. Less than 1dB amplitude and 10° phase differences are obtained with this method.

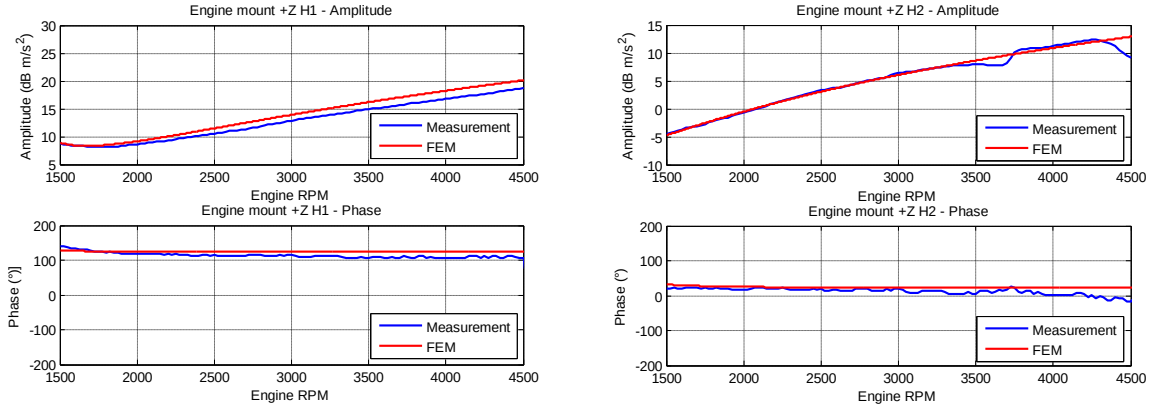

Fig. 16. Comparison between calculated and measured engine vibrations – Inertia harmonics.

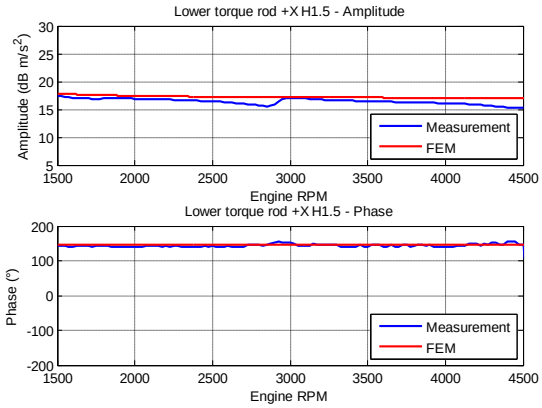

Fig. 17. Comparison between calculated and measured engine vibrations – Gas harmonics.

7 Conclusion

In this paper we presented a new efficient method to determine inertia properties of an automotive powertrain using few amounts of measurements. General equations of the method can be applied from 2-cylinders to 6-cylinders powertrains. This method was validated on a 3-cylinder powertrain, both by numerical tests and experimental tests showing accuracy.
Based on mechanics equations, this simple method allows determining main inertia properties of a powertrain with good precision. Compared to classical methods such as pendulum method or modal method, this new in situ method reduces instrumentation significantly and can be integrated into classical development validation phase to provide very early inertia properties to CAE development teams.

8 Acknowledgements

The authors sincerely thank the support of Renault NVH powertrain test team and especially S. Pallez and A. Rocher.

References

[1] D.J. Ewins, *Modal testing, Theory, Practice and Application*, Katholieke Universiteit Leuven, Departement Werktuigkunde, Leuven (1997).

[2] B. Swoboda, *Mécanique des moteurs alternatifs*, Publications de l'Institut Français du Pétrole (1984).

[3] Q.Leclère, L. Polac, B. Laulagnet, J-L. Guyader, *Vibro-acoustique des moteurs d'automobile*, Techniques de l'Ingénieur (2006).

[4] L.Polac, A.Anton, *A new efficient and accurate experimental method for estimating automotive powertrain inertia properties,* SAE (2009).

[5] S. Banazak, L. Duvermy, *détermination expérimentale des caractéristiques massiques d'un véhicule de tourisme,* SIA congrès de dynamique du véhicule – Centrale Lyon 9-10 juin 1999.

[6] J. Toivola, O. Nuutila. "*Comparison of three methods for determining rigid body inertia properties from frequency response functions*". Tempere University of Technology.

[7] H. Okuzumi. "*Identification of the rigid body characteristics of a powerplant by using experimental obtained transfer functions*". Ce laboratories, Nissan motor CO., Ltd., June 1991.

[8] Y. Gendry, *Détermination des valeurs d'inertie d'un GMP*, Course report august 2008